JEM Journal of Experimental Medicine

BRIEF DEFINITIVE REPORT

Regenerating murine CD8⁺ lung tissue resident memory T cells after targeted radiation exposure

Mariah Hassert[1], Lecia L. Pewe[1], Rui He[2], Mohammad Heidarian[1,3], Pornpoj Phruttiwanichakun[2], Stephanie van de Wall[1], Madison R. Mix[1,4,5], Aliasger K. Salem[2,4], Vladimir P. Badovinac[1,3,4]*, and John T. Harty[1,3,4]*

Radiation exposure occurs during medical procedures, nuclear accidents, or spaceflight, making effective medical countermeasures a public health priority. Naïve T cells are highly sensitive to radiation-induced depletion, although their numbers recover with time. Circulating memory CD8⁺ T cells are also depleted by radiation; however, their numbers do not recover. Critically, the impact of radiation exposure on tissue-resident memory T cells (T_{RM}) remains unknown. Here, we found that sublethal thorax-targeted radiation resulted in the rapid and prolonged numerical decline of influenza A virus (IAV)–specific lung T_{RM} in mice, but no decline in antigen-matched circulating memory T cells. Prolonged loss of lung T_{RM} was associated with decreased heterosubtypic immunity. Importantly, boosting with IAV-epitope expressing pathogens that replicate in the lungs or peripheral tissues or with a peripherally administered mRNA vaccine regenerated lung T_{RM} that was derived largely from circulating memory CD8⁺ T cells. Designing effective vaccination strategies to regenerate T_{RM} will be important in combating the immunological effects of radiation exposure.

Introduction

Ionizing radiation exposure can occur through several mechanisms—both intentional and unintentional. Ionizing radiation plays a central role in medical diagnosis and treatment. This can come in a range of exposures from low doses (e.g., x-ray imaging) to relatively high doses (e.g., tissue-targeted radiotherapy for cancer treatment or transplantation) (IEA-Reports, 2019; Slavin, 1987; Zhang et al., 2021). Ionizing radiation is high energy in the form of waves or particles that can damage biological material at even subcellular levels by the induction of direct or indirect DNA damage, as well as the initiation of inflammation (Cytlak et al., 2022). Radiation therapy is regarded as an attractive antitumor treatment because of its ability to induce death to the tumor cells and produce immunomodulatory effects that ensue within and surrounding the tumor following radiotherapy, termed abscopal responses (Cytlak et al., 2022; Galluzzi et al., 2017; Guipaud et al., 2018; Ukleja et al., 2021; Nabrinsky et al., 2022).

Memory T cells are an important immune cell subset in response to infection. Memory T cells are categorized into T central memory (T_{CM}), T effector memory (T_{EM}), and T resident memory (T_{RM}) based on their circulation patterns (Martin and Badovinac, 2018; Jameson and Masopust, 2018). The more recently described T_{RM} are lodged within tissues and do not typically recirculate (Mueller et al., 2013; Jiang et al., 2012; Gebhardt et al., 2009; Wakim et al., 2010). In tissues with an epithelioid structure (such as the lungs), CD8⁺ T_{RM} are defined as expressing the α E-integrin CD103 and the C-type lectin receptor CD69, both of which aid in tissue retention (Cepek et al., 1994; Casey et al., 2012; Masopust et al., 2001; Low and Kaech, 2018; Laidlaw et al., 2014). CD8⁺ lung T_{RM} are elicited following influenza virus infection and are important for strain-transcending heterosubtypic immunity (HI) to the strains of the virus where antibody-mediated elimination does not occur (Slütter et al., 2017; Liang et al., 1994; Wu et al., 2014).

Despite the extensive use of radiation technologies in medical treatment and diagnostics, as well as the increase in the use of radiation in the clean energy sector, relatively little is known about the effects of radiation on T cells—in particular memory T cells. As cells capable of rapid proliferation, naïve T cells are highly sensitive to radiation, although their numbers recover

[1]Department of Pathology, Carver College of Medicine, University of Iowa, Iowa City, IA, USA; [2]Department of Pharmaceutical Sciences and Experimental Therapeutics, College of Pharmacy, University of Iowa, Iowa City, IA, USA; [3]Department of Pathology Graduate Programs, Carver College of Medicine, University of Iowa, Iowa City, IA, USA; [4]Interdisciplinary Graduate Program in Immunology, Carver College of Medicine, University of Iowa, Iowa City, IA, USA; [5]Medical Scientist Training Program, University of Iowa, Iowa City, IA, USA.

Correspondence to John T. Harty: john-harty@uiowa.edu

*V.P. Badovinac and J.T. Harty are co-senior authors.

© 2024 Hassert et al. This article is distributed under the terms of an Attribution–Noncommercial–Share Alike–No Mirror Sites license for the first six months after the publication date (see http://www.rupress.org/terms/). After six months it is available under a Creative Commons License (Attribution–Noncommercial–Share Alike 4.0 International license, as described at https://creativecommons.org/licenses/by-nc-sa/4.0/).

with time (Grayson et al., 2002). A study published in 2002 examined the effects of ionizing radiation on naïve and memory CD8⁺ T cells following radiation exposure (Grayson et al., 2002). This study found that naïve T cells are highly sensitive to acute radiation-induced death, whereas memory CD8⁺ T cells are relatively more resistant (Grayson et al., 2002). While this study did offer insight on the acute impact of radiation on memory CD8⁺ T cells, it remained unclear until recently, the long-term effects of radiation exposure on memory T cells. To address this, we recently described the long-term impact of sublethal total body irradiation on circulating memory T cells (Heidarian et al., 2023). In addition to being numerically depleted following radiation exposure, circulating memory T cell numbers do not recover with time, unlike naïve T cells. Interestingly, the few circulating memory T cells that survive radiation exposure exhibit reduced antigen sensitivity and decreased proliferative responses to antigen re-exposure, resulting in a loss of bacterial control in a subsequent *Listeria* challenge. Thus, sublethal whole-body radiation exposure has long-term deleterious effects on both the number and function of circulating memory T cells. However, despite being a critically protective subset in response to tissue-specific infections, it is unclear how T_{RM} are affected by radiation exposure. In the current study, we utilized well-characterized models of influenza A virus (IAV)–induced lung T_{RM} generation (Slütter et al., 2017; Low et al., 2020) to study the impact of thorax-targeted radiation exposure on lung T_{RM} maintenance and regeneration. We ultimately found that T_{RM} are sensitive to radiation-induced loss following thorax-targeted irradiation while circulating memory T cells are preserved and can be boosted to regenerate lung T_{RM}.

Results and discussion

Thorax-targeted irradiation results in long-term numerical loss of lung T_{RM} while maintaining peripheral memory populations

We recently showed that that exposure of immune mice to 5 Gray (Gy) of whole-body irradiation results in a lasting numerical decline in circulating memory CD8⁺ T cells and a reduction in their functionality and antigen sensitivity (Heidarian et al., 2023). Given these findings, we deemed it important to investigate the impact of targeted radiation exposure on lung T_{RM} in an established model of murine influenza infection. To address this, we utilized an established C57BL/6 model of IAV infection, which has previously been demonstrated to elicit a robust, virus-specific lung CD8⁺ T_{RM} response that is necessary for HI (Liang et al., 1994; Slütter et al., 2017). In this approach, we used IAV expressing the H-D^b restricted lymphocytic choriomeningitis virus (LCMV) epitope GP_{33-41} epitope (GP33) in conjunction with trackable P14 T cell receptor transgenic T cells specific for the LCMV GP33 epitope (Mueller et al., 2010). 20,000 Thy 1-disparate P14 cells were transferred into C57BL/6 mice 1 day prior to sublethal intranasal infection (IN) with the mouse-adapted H1N1 influenza virus PR8 expressing GP_{33} (PR8-GP33) (Mueller et al., 2010). To optimize the dose of radiation, 30 days following infection, mice were sublethally irradiated with 2, 5, or 10 Gy targeted to the thorax through the use of an Xstrahl Small Animal Radiation Research Platform (SARRP), which permits the targeting of x-ray beams using computerized tomography (CT) image guidance. At day 13 after radiation exposure, lymphocytes were harvested from the lungs (Fig. 1 A). To distinguish cells in the circulation from those in the tissues, an intravascular (IV) CD45.2 stain was administered prior to euthanasia (Fig. S1 A) (Slütter et al., 2017; Anthony et al., 2021; Van Braeckel-Budimir et al., 2018).

At 13 days post radiation (DPR) exposure, we observed a slight, though not statistically significant, reduction in total IV-negative CD8⁺ T cells in the lungs of irradiated mice, particularly, at the 10 Gy dose (Fig. 1 B). When examining IV-negative P14 cells in the lungs, we observed a dose-dependent reduction of cells in response to radiation exposure, with the most robust reduction in P14 cells being observed at the 10 Gy dose and 2 Gy being not sufficient to result in a statistically significant reduction of P14 cells (Fig. 1 C). Interestingly, we observed a profound numerical reduction of P14 lung T_{RM} (CD103⁺ CD69⁺) in response to both 5 and 10 Gy of radiation exposure (Fig. 1 D). As CD4⁺ T cells have also been demonstrated to play a role in protection from IAV (Teijaro et al., 2010; Brown et al., 2006), we also measured the effects of radiation exposure on this population. We observed a slight reduction in IV-negative CD4⁺ T cells that was statistically significant at the 10 Gy dose (Fig. 1 E). We examined IV-negative cells specific to the I-A^b restricted IAV epitope NP_{311} by tetramer staining and similarly observed a radiation dose-dependent numerical reduction (Fig. 1 F). To determine the effects of radiation exposure on CD4⁺ T_{RM}, we gated on NP_{311} tetramer-positive cells that were CD69⁺ (Teijaro et al., 2010). We observed a statistically significant reduction in CD4⁺ lung T_{RM} at the 10 Gy dose (Fig. 1 G). Due to the clearest phenotype being observed at the 10 Gy dose and the dose having been previously utilized to model radiotherapy of lung cancer (Kirsch et al., 2010; Fakiris et al., 2009; Perez et al., 2013), we opted to proceed with the 10 Gy dose. As previous studies have demonstrated the importance of CD8⁺ T_{RM} in HI from IAV (Slütter et al., 2017; Wu et al., 2014), and our lab possesses the tools and expertise to rigorously study these cells, we opted to perform a more in-depth analysis on the effects of radiation on this subset.

To determine the kinetics of radiation-induced lung T_{RM} depletion, we harvested lymphocytes from the lungs on days 3, 13, and 34 after radiation exposure to enumerate and phenotype the memory T cell subsets (Fig. 1 A) (Fig. S1). Bulk IV-negative CD8⁺ T cells were transiently reduced by 13 DPR and subsequently recovered (Fig. 1 H). Of those IV-negative CD8⁺ T cells, we found that there was a trending reduction in total memory P14 cells in the lungs by day 3 after radiation exposure that increased significantly (5.9× reduction in 10 Gy versus 0 Gy) by 13 DPR but ultimately equilibrated by 34 DPR (Fig. 1 I). Consistent with our earlier experiments, we found a statistically significant reduction (~21×) in the total numbers of lung CD103⁺CD69⁺ P14 T_{RM} that was apparent by day 13 after radiation exposure and sustained out to day 34 (Fig. 1 J). These data demonstrated that lung T_{RM} were deleted and failed to numerically recover after thorax-targeted radiation exposure (Fig. 1 K).

Because the lung is a highly vascularized organ that contains many circulating T cell populations (Hassert and Harty, 2022;

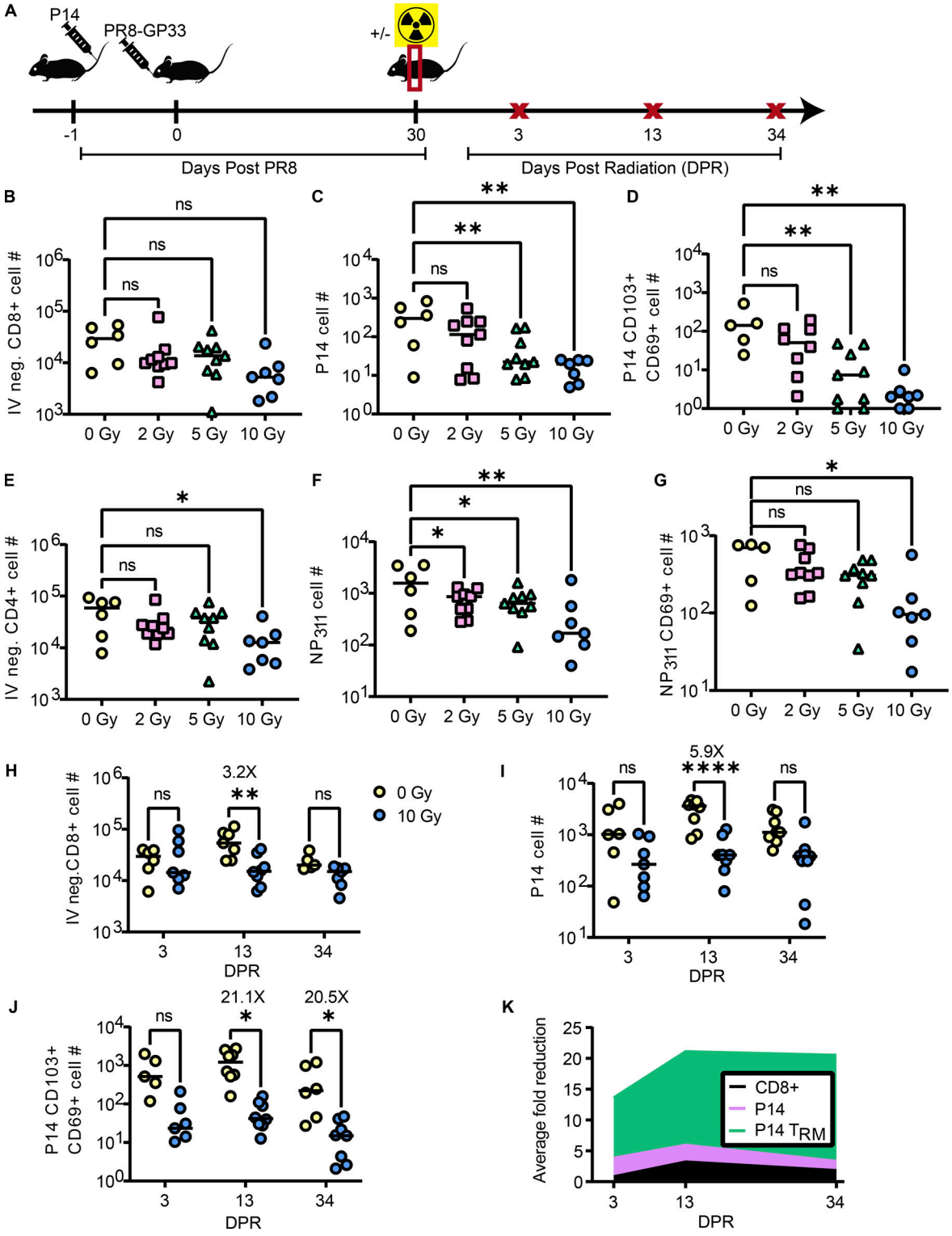

Figure 1. **Thorax-targeted radiation exposure results in long-term numerical loss of lung T_{RM} while maintaining peripheral CD8⁺ T memory populations. (A)** Experimental schematic to determine the effects of tissue-targeted irradiation on lung T_{RM}. Mice were administered P14 1 day prior to infection with PR8-GP33. 30 days post primary infection (DPPI), a subset of mice were exposed to thorax-targeted radiation or treated similarly without radiation exposure. At 3, 13, and 34 DPR, a subset of mice from each group were euthanized and lungs and spleen cells were analyzed by flow cytometry. **(B–G)** At 13 DPR, total numbers of (B) IV-negative CD8⁺ T cells in the lungs, (C) IV-negative P14 cells in the lungs, (D) CD69⁺CD103⁺ P14 lung T_{RM}, (E) IV-negative CD4⁺ T cells, (F) IV-negative NP_{311} tetramer–positive cells, and (G) CD69⁺ NP_{311} tetramer–positive T_{RM} were quantified. **(H–J)** At 3, 13, and 34 days after 10 Gy radiation exposure, total numbers of (H) IV-negative CD8⁺ T cells in the lungs, (I) IV-negative P14 cells in the lungs, and (J) CD69⁺CD103⁺ P14 lung T_{RM} were quantified. **(K)** The average fold difference in the total numbers of IV-negative CD8⁺ T cells, P14 cells, and P14 T_{RM} was quantified over time. ANOVA was utilized to determine statistically significant differences between groups. Data are pooled from two independent experiments (n = 6–7 mice per group). Statistical significance has been indicated within the figures with asterisks (*P = 0.03, **P = 0.002, ****P < 0.0001).

Jameson and Masopust, 2018), we also assessed peripheral memory T cell responses after radiation exposure (Fig. S1 B). Mice that underwent thorax-targeted radiation exposure had equivalent total CD8⁺ T cells (Fig. S1 C), P14 cells (Fig. S1 D), T_{CM} (Fig. S1 E), and T_{EM} (Fig. S1 F) in the spleen at all time points assessed. This indicated that despite a pronounced and long-lived effect of thorax-targeted radiation exposure on lung T_{RM}, the peripheral memory CD8⁺ T cell compartment remained numerically intact.

Radiation-induced loss of T_{RM} in the lung results in compromised HI to influenza

T_{RM} have been demonstrated to be critical for protection against a number of life-threatening pathogens (Liang et al., 1994; Slütter et al., 2017; Luangrath et al., 2021; Fernandez-Ruiz et al., 2016; Sakai et al., 2014). This finding implies that targeted radiation exposure (perhaps from medical treatment for cancer or accidental exposure) has the potential to compromise vaccine or infection-induced tissue resident immunity. Importantly, it has been demonstrated that when lung T_{RM} wanes with time after IAV infection, HI is lost—showing that these populations are critical for HI to IAV infection (Slütter et al., 2017; Liang et al., 1994). Therefore, we predicted that a loss of IAV-specific lung T_{RM} following thorax-targeted radiation exposure would compromise HI to IAV. To address this, we immunized C57BL/6 mice with a sublethal infection of the H3N2 murine-adapted influenza X31-GP33, which expressed conserved CD8⁺ T cell epitopes with PR8-GP33 but different hemagglutinin and neuraminidase subtypes (Yewdell et al., 1985). 30 DPR, the mice underwent heterosubtypic challenge via IN inoculation of a $5LD_{50}$ dose of PR8-GP33 (Fig. 2 A).

Consistent with previous studies, mice began to lose weight at 4 days post infection (DPI) with PR8-GP33 (Fig. 2 B) (Rutigliano et al., 2014). Mice that had no prior X31-GP33 infection trended to lose slightly more weight than mice with prior influenza exposure. Radiation exposure did not measurably impact weight loss up to 4 DPI. Mice with no prior X31-GP33 exposure had robust viral replication that was detected in both the bronchoalveolar lavage (BAL) fluid and lung tissue after euthanasia at 4 DPI (Fig. 2, C and D). Importantly, there were no detectable differences in viral titers in mice with no prior IAV exposure in the presence or absence of thorax-targeted radiation, indicating that radiation exposure does not impact overall acute IAV susceptibility in naïve animals. Prior exposure to X31-GP33 led to substantial protection from viral replication as indicated by a ∼100× drop in viral titers in the lungs and ∼1,000× drop in the BAL fluid, consistent with previous studies (Fig. 2, C and D) (Slütter et al., 2017). However, X31-GP33 immune mice exposed to thorax-targeted radiation had substantially higher viral titers in the lungs and BAL after PR8-GP33 challenge compared with their non-irradiated counterparts. This finding was consistent with prior studies indicating that lung T_{RM} are critical in protection from heterosubtypic IAV challenge (Slütter et al., 2017). Thus, the specific loss of lung T_{RM} following thorax-targeted radiation exposure precluded optimal HI. Due to the importance of both CD8⁺ and CD4⁺ T_{RM} in HI to IAV, this compromised HI to IAV is likely the result of the loss of both subsets. This pathological significance underscores the importance of the development of strategies to counteract tissue-specific effects of radiation exposure on local host defense.

Regeneration of lung T_{RM} by boosting

We demonstrated that lung T_{RM} loss following radiation exposure had consequences for HI during IAV infection (Fig. 2). In contrast to whole-body radiation exposure (Heidarian et al., 2023), thorax-targeted irradiation did not reduce peripheral memory T cell numbers (Fig. S1, C–F). Therefore, peripheral memory T cells represent a potential source of memory cells that could be boosted and recruited to the lungs to rectify radiation-induced T_{RM} loss. To determine if the lung can be repopulated with T_{RM} following thorax-targeted radiation, X31-GP33 immune mice with or without thorax-targeted radiation exposure were boosted with a sublethal PR8-GP33 infection such that the effects on T_{RM} could be evaluated (Fig. 3 A).

Boosting IN with PR8-GP33 resulted in a statistically significant increase of IV-negative CD8⁺ T cells particularly in the lungs of irradiated mice (4.4×) (Fig. 3 B). Similarly, we observed significant increases of IV-negative P14 cells in boosted mice with previous radiation exposure (Fig. 3 C). This boosting was also observed in non-irradiated mice, though interestingly, the increase was much more robust in mice with radiation exposure (73.7× versus 3.8×). Of the IV-negative P14 cells, there was a substantial increase in T_{RM} in the lungs of boosted irradiated mice (Fig. 3 D). Irradiated mice had more robust increases of T_{RM} following boosting compared with non-irradiate mice (597× versus ∼5×). The mechanism for such robust antigen-specific T_{RM} boosting is unclear but warrants further investigation. We hypothesize that radiation exposure in the context of prior IAV experience may result in additional antigen release, driving an enhanced T_{RM} boosting. In the spleens of these vaccinated mice, we did not observe any statistically significant changes in overall CD8⁺ T cell numbers (Fig. 3 E). However, with respect to memory P14 cells in the spleen, we observed an increase in P14 cells after boosting irradiated mice (Fig. 3 F). Similar to the lung tissue, the efficiency of boosting was enhanced in irradiated hosts. When splenic memory P14 cells were further subsetted into T_{CM} and T_{EM}, we observed that boosting did not lead to a substantial increase of T_{CM} (Fig. 3 G) but a significant increase in T_{EM}, accounting for the majority of increased P14 cells following boost (Fig. 3 H). Together, these data demonstrated that IN boosting with PR8-GP33 resulted in the regeneration of IAV-specific T_{RM} that were lost due to radiation exposure.

Newly recruited T_{RM} are derived from peripheral memory T cells

Local antigen exposure induced recovery of lung T_{RM} following their radiation-induced depletion (Fig. 3). However, the source of these new T_{RM} recruits was unknown. Due to the numerical retention of circulating memory T cells following thorax-targeted radiation exposure, we hypothesized that the influx of circulating memory T cells and subsequent T_{RM} conversion could be the source of the new lung T_{RM} in the context of radiation exposure and boost. To address this issue, we specifically depleted circulating memory P14 cells prior to boosting with a

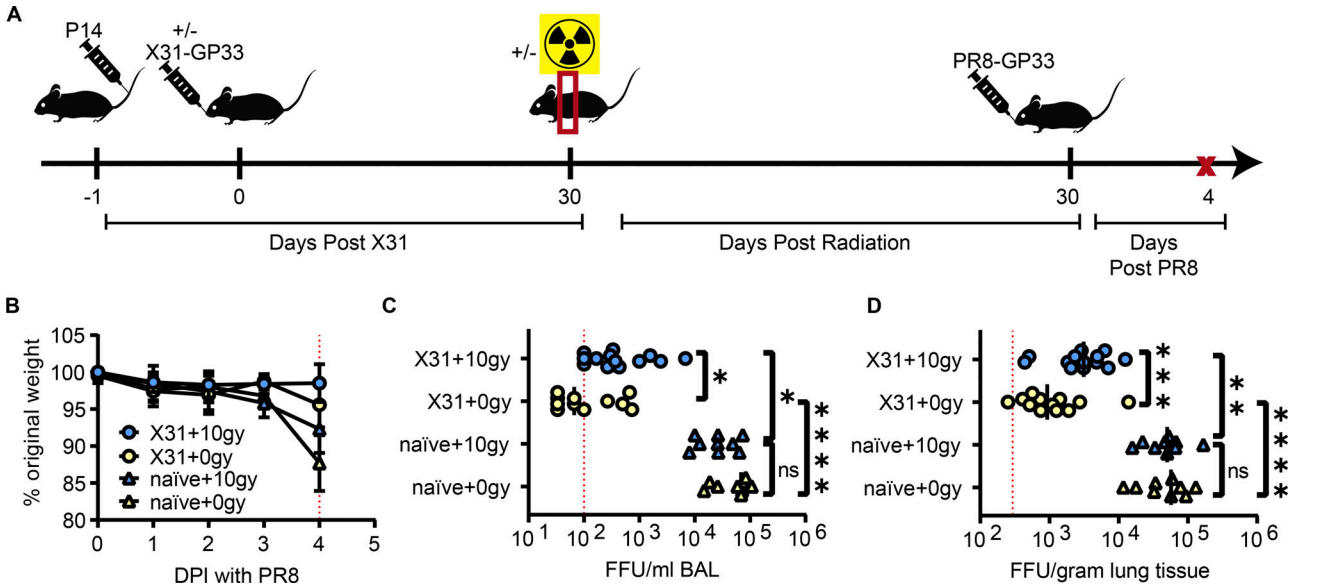

Figure 2. **Radiation-induced loss of T_{RM} in the lung results in compromised heterosubtypic immunity to influenza virus. (A)** Experimental schematic to determine the effects of thorax-targeted radiation exposure on IAV susceptibility. Mice were administered P14 1 day prior to infection of half of the mice with X31-GP33. 30 days after X31 infection, half of the mice were exposed to 10 Gy of thorax-targeted radiation or treated similarly without radiation exposure. 30 DPR, mice were infected IN with $5LD_{50}$ of PR8-GP33. On day 4 after PR8 infection, mice were euthanized, and BAL and lung viral titers were measured via FFA. **(B)** Mice were weighed for 4 days following lethal PR8-GP33 challenge. **(C)** BAL PR8-GP33 titers on day 4. **(D)** Lung PR8-GP33 titers on day 4. ANOVA was utilized to determine statistically significant differences between groups. Data are pooled from two independent experiments (n = 9–13 mice per group). Statistical significance has been indicated within the figures with asterisks (*P = 0.03, **P = 0.002, ***P = 0.0002, ****P < 0.0001).

sublethal dose of PR8-GP33 (Fig. 4 A). Prior to boosting, we confirmed that the anti-CD90.1 antibody dose was sufficient to deplete circulating P14 cells but not T_{RM} P14 cells (Fig. S2).

We found no statistically significant differences in the total number of IV-negative lung $CD8^+$ T cells between isotype and mice treated with anti-CD90.1 (Fig. 4 B). However, we found that mice depleted of circulating P14 cells prior to boosting had a significant reduction in both IV-negative lung P14 (Fig. 4 C) and P14 T_{RM} (Fig. 4 D) (~7×). Upon examining T cells from the spleens of these mice, we found no statistically significant differences in the total number of $CD8^+$ T cells (Fig. 4 E). However, we observed a statistically significant reduction in P14 cells among mice treated with anti-CD90.1 (Fig. 4 F) (7.3×). This difference was conserved when memory P14 cells were subsetted into both T_{CM} and T_{EM} populations (Fig. 4, G and H). These data demonstrated that depletion of circulating memory T cells prior to boosting prevented regeneration of lung T_{RM} lost during thorax-targeted radiation exposure. This suggested that circulating memory T cells were precursors for the regeneration of T_{RM} after radiation-induced depletion and subsequent IAV boost.

How new T_{RM} recruits are generated in different tissues is an active area of investigation, with tissue occupying T_{RM} and/or CD69 single-positive T cells, being put forth as precursor candidates (Kok et al., 2022). Our peripheral P14 depletion results support a major role for circulating memory cells as a source for new T_{RM} following antigen re-exposure, at least in mice where lung T_{RM} were depleted by thorax-targeted radiation. A limitation of this study includes the fact that mediastinal lymph nodes (mLN) could not be recovered from irradiated animals likely due to damage from radiation exposure. Therefore, the relative contributions of mLN to the recovery of lung T_{RM} cannot be excluded.

Intramuscular mRNA vaccination has the potential to be utilized as a strategy to re-invigorate lung T_{RM}

In a previous study, we found that the utilization of a peripheral boosting strategy (*Listeria monocytogenes* [LM] expressing GP_{33}) (LM-GP33) administered intravenously could function to re-invigorate lung T_{RM} following their natural waning over time (Slütter et al., 2017). LM-GP33 infection does not on its own generate any bona fide $CD103^+$ $CD69^+$ lung T_{RM} (Slütter et al., 2017). Those prior studies demonstrated that both local and non-tissue-localized antigen exposure could serve to reinvigorate lung T_{RM}. To determine if peripheral boosting could regenerate lung T_{RM} previously lost to radiation exposure, we repeated this LM boosting strategy in the context of prior thorax-targeted radiation exposure. 30 days after boost, we observed a significant increase in IV-negative P14 cells in mice immunized with LM-GP33 relative to those vaccinated with an LM expressing an irrelevant *Plasmodium* epitope from the glideosome 50 (Gap50) protein (LM-Gap50) (Fig. S3 A) and a statistically significant increase in P14 T_{RM} (Fig. S3 B), indicating that this peripheral reinvigoration strategy could be effective in the context of prior radiation-induced T_{RM} depletion.

This LM-GP33 peripheral boosting experiment served as a proof-of-principal approach to demonstrate that peripheral antigen could indeed reinvigorate lung T_{RM} following thorax-targeted irradiation. However, this method is limited with respect to clinical feasibility. The use of mRNA vaccines to combat

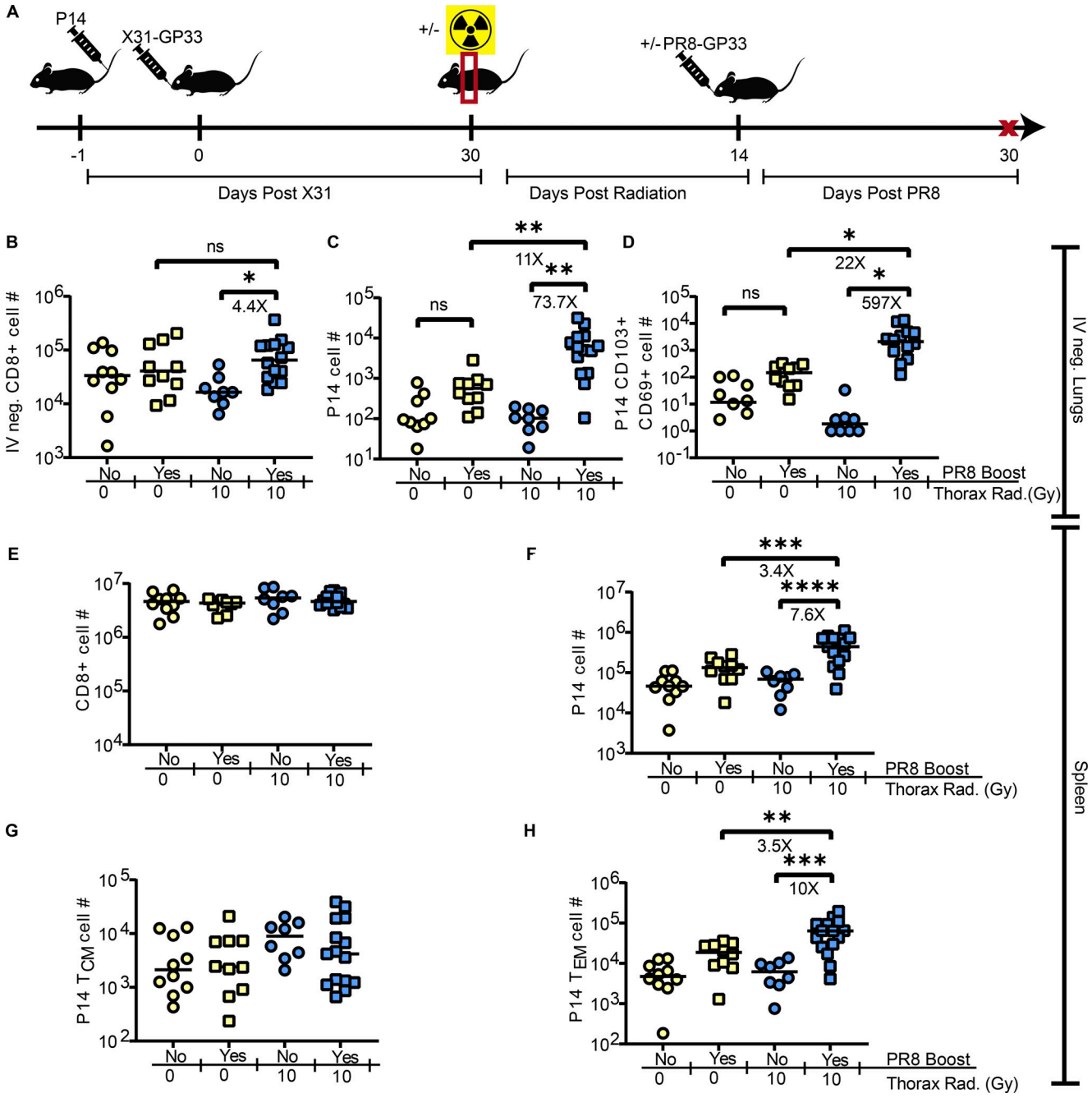

Figure 3. **Intervention to regenerate T_{RM} populations after radiation-induced loss. (A)** Experimental schematic. Mice were administered P14 cells 1 day prior to infection of half of the mice with X31-GP33. 30 DPPI, half of the mice were exposed to 10 Gy of thorax-targeted radiation or treated similarly without radiation exposure. 14 DPR, mice were infected IN with a sublethal PR8-GP33 boost or PBS as a control. 30 days later, mice were euthanized and lungs and spleen cells were analyzed by flow cytometry. **(B–H)** Flow cytometric analysis was utilized to count the total number of (B) IV-negative $CD8^+$ T cells in the lungs, (C) IV-negative P14 cells in the lungs, (D) $CD69^+CD103^+$ P14 lung T_{RM}. In the same mice, flow cytometric analysis was utilized on whole spleens to enumerate the total number of (E) $CD8^+$ T cells, (F) P14 cells, (G) T_{CM} P14 cells, and (H) T_{EM} P14 cells. ANOVA was utilized to determine statistically significant differences between groups. Data are pooled from three independent experiments (n = 9–15 mice per group). Statistical significance has been indicated within the figures with asterisks (*P = 0.03, **P = 0.002, ***P = 0.0002, ****P < 0.0001).

the COVID-19 pandemic represented a novel and adaptable strategy for rapid vaccine development in emergency situations. We hypothesized that this could be a viable medical countermeasure to reinvigorate lung T_{RM} following local radiation exposure. To this end, we designed a first-generation mRNA vaccine termed "Ub-Flu" to elicit $CD8^+$ T cell responses against NP_{366}, PA_{224}, and GP_{33} by targeting the encoded polyprotein to the proteasome with an encoded ubiquitin tag for more efficient MHC class 1 antigen processing (Fig. 5 A). 14 days after thorax-targeted irradiation, mice were immunized via the intramuscular route (IM) with this RNA vaccine (Fig. 5 B). We confirmed immunogenicity by collecting peripheral blood lymphocytes at

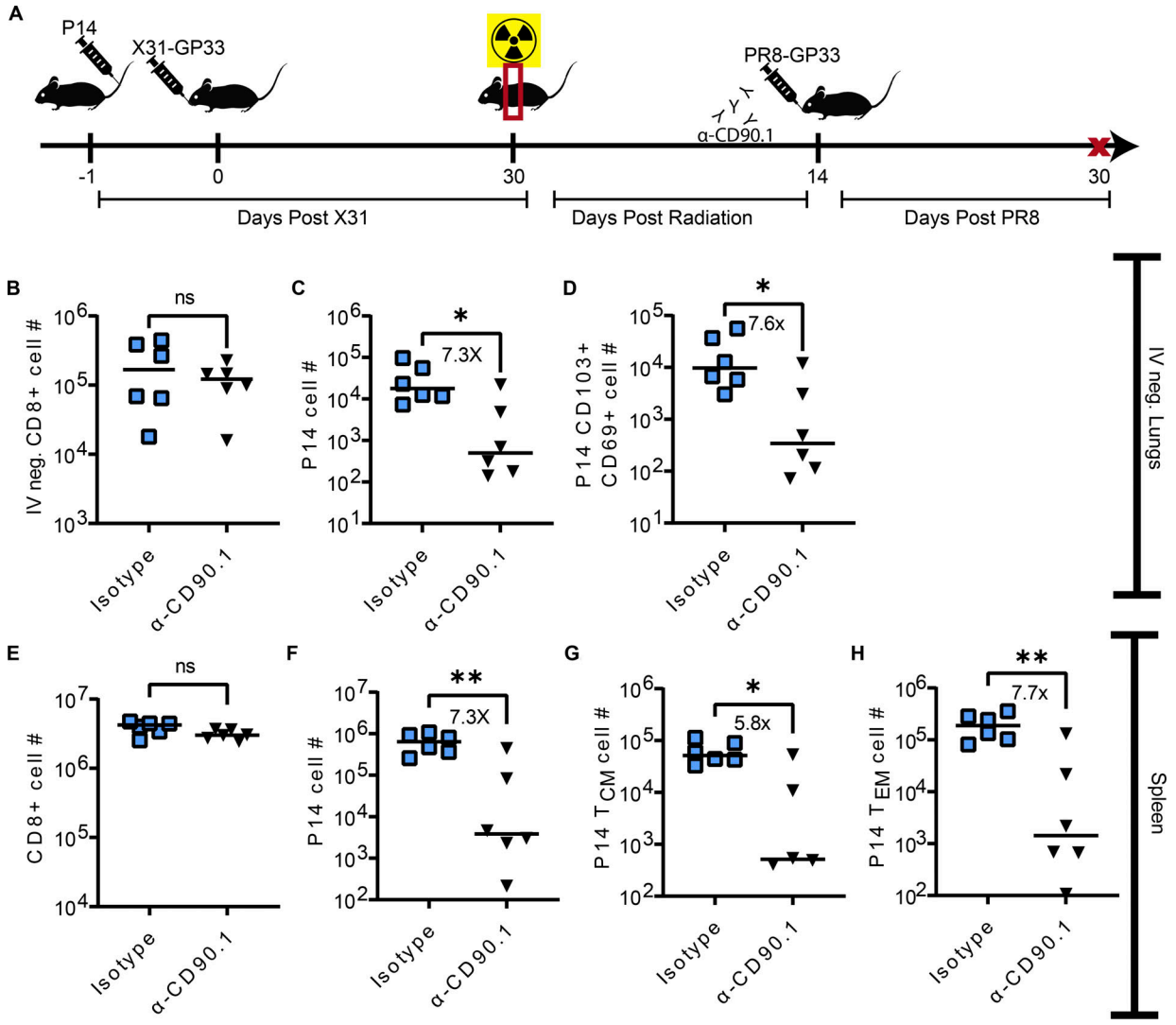

Figure 4. **Many newly recruited T_{RM} are derived from peripheral memory T cells. (A)** Experimental design. Mice were administered P14 1 day prior to infection with X31-GP33. 30 DPPI, all of the mice were exposed to 10 Gy of thorax-targeted radiation. 14 DPR, half of the mice were administered an anti-CD90.1 to deplete circulating Thy1.1 P14 or isotype control antibodies. Mice were then infected IN with a sublethal PR8-GP33 boost. 30 days later, mice were euthanized, and lungs and spleens were analyzed by flow cytometry. **(B–H)** Flow cytometric analysis was utilized to count the total number of (B) IV-negative $CD8^+$ T cells in the lungs, (C) IV-negative P14 cells in the lungs, and (D) $CD69^+CD103^+$ P14 lung T_{RM}. In the same mice, flow cytometric analysis was utilized on whole spleens to enumerate the total number of (E) $CD8^+$ T cells, (F) P14 cells, (G) T_{CM} P14 cells, and (H) T_{EM} P14 cells. Mann–Whitney test was utilized to determine statistically significant differences between groups. The data are pooled from two independent experiments (n = 6 mice per group). Statistical significance has been indicated within the figures with asterisks (*P = 0.03, **P = 0.002).

day 7 after vaccination and identifying P14 effector T cells by flow cytometry (Fig. 5 C). At this effector time point, an average of 18% of $CD8^+$ T cells in the blood of vaccinated mice were P14 cells, indicating a robust peripheral antigen-specific boosting.

At 30 days after vaccination, lungs and spleens were harvested to determine the impact of antigen-specific mRNA boosting on lung T_{RM} in mice that had received radiation exposure. Antigen-specific mRNA vaccination did not lead to a statistically significant increase in IV-negative total $CD8^+$ T cells in the lungs compared with irrelevant vaccine control (GFP-Scram) (Fig. 5 D). However, consistent with the LM peripheral infection system, peripheral antigen-specific mRNA boosting led to an increase in IV-negative P14 cells in the lung (Fig. 5 E) (7.6×) and P14 T_{RM} (Fig. 5 F) (8.2×). Upon analysis of splenocytes from irradiated and vaccinated mice, we saw no statistically significant increase in total $CD8^+$ T cells in Ub-Flu–vaccinated mice compared with irrelevant control mice (Fig. 5 G). However, we observed an increase in total P14 cells in the spleen (Fig. 5 H) (5.3×). When we subset these P14 cells into T_{CM} (Fig. 5 I) and T_{EM} (Fig. 5 J), we found no change in the number of P14 cells that were T_{CM} in Ub-Flu–vaccinated mice. However, there was a statistically significant increase of T_{EM} in Ub-Flu–vaccinated mice relative to control mice (7.9×). These findings indicated that mRNA vaccination could function to reinvigorate T_{RM} in the lung previously lost to targeted radiation exposure likely via recruitment and conversion of peripheral memory T cells.

Boosting IAV-immunized mice with thorax-targeted radiation exposure with IN PR8-GP33, IV LM-GP33 infection, or IM

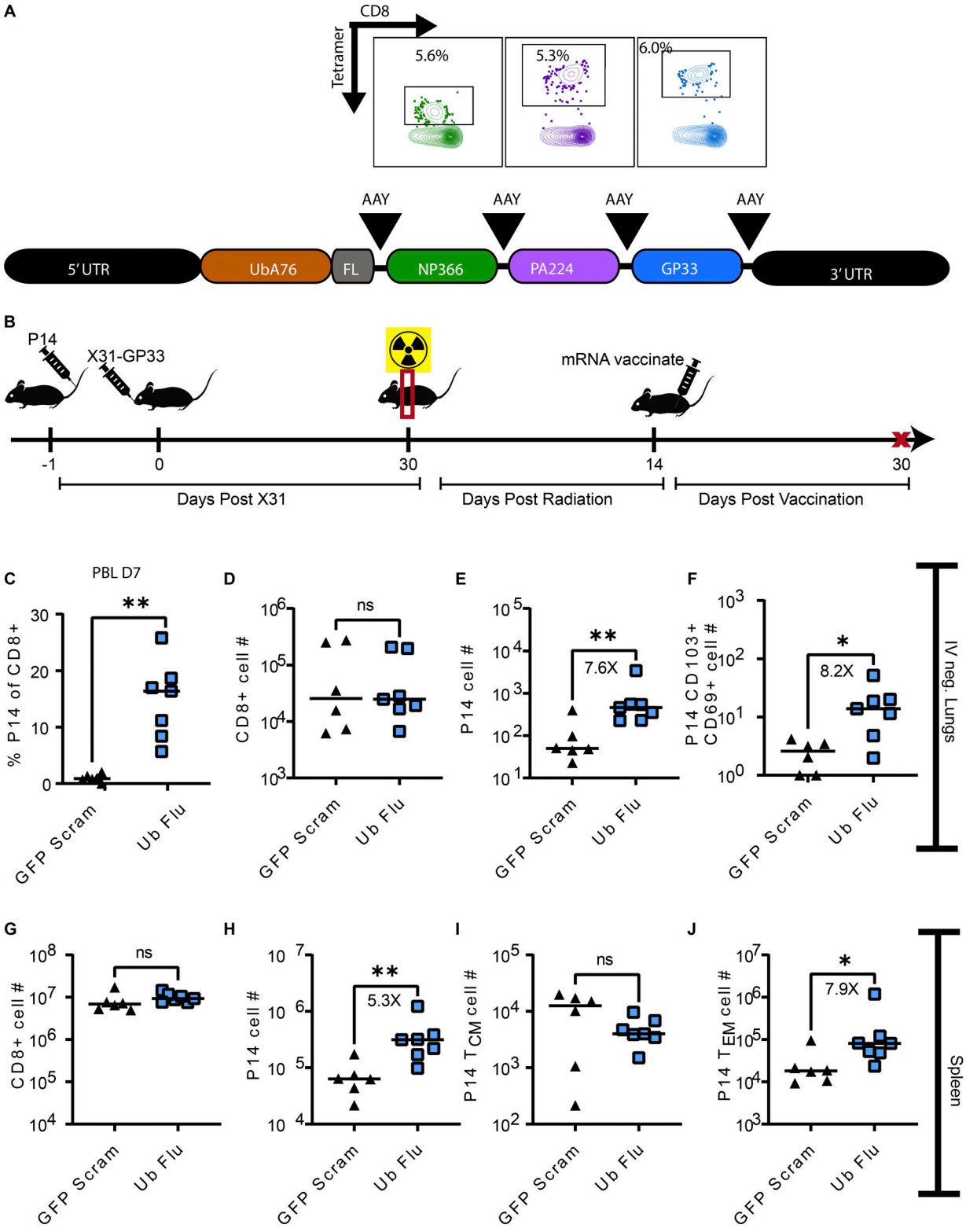

Figure 5. **Intramuscular mRNA vaccination can re-invigorate lung T_{RM}. (A)** mRNA vaccine design for Ub-Flu first generation vaccine. Following the 5′ UTR, a mutant ubiquitin is encoded which cannot be cleaved. Immediately 3′ to the ubiquitin is a flexible linker, followed by the coding sequence for NP_{366}, PA_{224}, and GP_{33} epitopes all flanked by AAY (alanine, alanine, tyrosine) optimal proteasomal cleavage sites. Representative flow plots of a B6 mouse immunized with 5 µg IM route demonstrate induction of $CD8^+$ T cells specific to NP_{366} (green), PA_{224} (purple), or GP_{33} (blue) 7 days following a single immunization. **(B)** Mice were administered P14 1 day prior to infection with X31-GP33. 30 days after X31 infection, all of the mice were exposed to 10 Gy of thorax-targeted radiation. 30 DPR, mice were immunized IM with 5 µg of either the relevant construct, or a similar construct encoding GFP and a nucleotide scrambled version of the same epitopes. 7 days after boost, peripheral blood was collected and stained to identify P14 T cells. 30 days after boost, mice were euthanized, and lungs and spleen cells were analyzed by flow cytometry. **(C)** Confirmation of immunogenicity 7 days after vaccination. Peripheral blood lymphocytes (PBL) were collected and

stained to enumerate the frequency of CD8⁺ T cells that were P14 cells. **(D–J)** Flow cytometric analysis was utilized to count the total number of (D) IV-negative CD8⁺ T cells in the lungs, (E) IV-negative P14 cells in the lungs, and (F) CD69⁺CD103⁺ P14 lung T_{RM}. In the same mice, flow cytometric analysis was utilized on whole spleens to enumerate the total number of (G) CD8⁺ T cells, (H) P14 cells, (I) T_{CM} P14 cells, and (J) T_{EM} P14 cells. Mann–Whitney test was utilized to determine statistically significant differences between groups (n = 6–7 mice per group). Statistical significance has been indicated within the figures with asterisks (*P = 0.03, **P = 0.002).

vaccination with a first-generation T cell–based mRNA vaccine resulted in varying degrees of regeneration of lung T_{RM}. Clearly, IN PR8-GP33 infection was the most efficient in regenerating lung T_{RM}. While an increase in lung T_{RM} was observed in irradiated Ub-Flu–boosted mice, this increase would ideally be larger, indicating that further optimization of this approach is warranted. It is possible that local administration of an mRNA vaccine or targeting lipid nanoparticles (LNPs) to specific APC subsets via inclusion of targeting antibodies in the LNP particle could drive an even more robust recruitment and conversion of peripheral memory cells to lung $T_{RM,}$ which we are currently investigating.

In summary, we defined the impact of tissue-targeted radiation exposure on CD4⁺ and CD8⁺ lung T_{RM}. We determined that lung T_{RM} are sensitive to radiation-induced depletion. Where total IV-negative CD8⁺ T cells in the lung eventually rebound, bona fide T_{RM} do not recover at least as far as 60 DPR. We found multiple boosting strategies, including local antigen administration or peripheral boosting with LM or an mRNA vaccine were capable of regenerating lung T_{RM} after restimulation of circulating memory T cells. These findings demonstrate that localized radiation exposure compromised the tissue residing memory T cell compartment but suggest vaccination as a potential medical countermeasure to rectify this defect.

Materials and methods

Ethics statement

All animal studies were done in accordance with the Guide for Care and Use of Laboratory Animals of the National Institutes of Health (NIH) and approved by the University of Iowa Animal Care and Use Committee (protocol #0051102).

Viruses and cells

The murine influenza H1N1 strain PR8 encoding the LCMV epitope GP_{33} and the H3N2 strain X31 encoding GP_{33} were obtained from Steven Varga (University of Iowa, Iowa City, IA, USA) via E. John Wherry (University of Pennsylvania, Philadelphia, PA, USA) and propagated in embryonated chicken eggs as previously described (Brauer and Chen, 2015). The titer of each viral stock was determined by focus-forming assay (FFA) on Madin-Darby canine kidney (MDCK) cells (Brien et al., 2019).

Mice and infections

6–8-wk old C57BL/6 mice were purchased from Charles River Laboratories and housed under specific pathogen–free conditions for the duration of the studies at the University of Iowa. 1 day prior to each infection, 20,000 P14 CD8⁺ T cells were administered to each mouse IV. For influenza infections, mice were anesthetized with a ketamine/xylazine cocktail prior to intranasal administration of a 25 µl bolus of virus (10 focus-forming units [FFU] of PR8 and 10^3 FFU of X31 for sublethal infection or boost and 7.5×10^2 FFU of PR8 for $5LD_{50}$ challenge). For LM-GP33 infections, mice were infected IV with 10^7 CFU per mouse.

Radiation exposure

For thorax-targeted radiation exposure, mice were anesthetized with isoflurane to undergo CT scanning to identify the region of interest and dosimetry followed by thorax-targeted irradiation using an Xstrahl SARRP. Non-irradiated controls were placed under isoflurane for an equivalent amount of time. Following radiation exposure, mice (and non-irradiated controls) were placed on an irradiated chow (cat. #7913; Envigo) for the remainder of the study to limit irrelevant infections.

Flow cytometry

3 min prior to euthanasia, mice were administered intravenous anti-CD45.2 (BV421) to label circulating lymphocytes. Lungs were harvested into a digestion media containing PBS, 0.05% collagenase, and 10 µg/ml DNase and incubated by shaking at 37°C for 1 h. Spleens were harvested into complete RPMI. Following digestion, tissues were homogenized and strained over a 100-µm filter. Lungs were further purified by centrifugation for 30 min at 1,200 × g at 4°C with no brake in a 30% Percoll gradient as previously described (Wilk et al., 2017). Red blood cells were lysed from each sample using Vitalyse according to the manufacturer's instructions (catalog #WBL0100; CMDG). Cell suspensions were stained with the following panel to identify T_{RM}: CD45.2 (BV421 IV stain), CD8α (APC), CD69 (PE Cy7), CD103 (PE), CD90.1 (PerCP Cy5.5), CD11a (AF488), and Viability dye (Efluor 780). Cell suspensions were stained with the following panel to identify T_{EM} and T_{CM}: CD45.2 (BV421 IV stain), CD8α (BV785), CD11a (AF488), CD62L (APC), CD90.1 (PerCP Cy5.5), and CD27 (PE). Cells were analyzed via flow cytometry using a BD Fortessa, and data were analyzed by FlowJo.

Measurement of viral burden

4 days following a $5LD_{50}$ PR8-GP33 infection, mice were euthanized and 1 ml of BAL fluid was collected on ice. Lung tissue was collected, weighed, and homogenized using a Thermo Fisher Scientific bead mill in 1 ml of DMEM. Following homogenization, tissues were centrifuged for 10 min and the supernatants were transferred to a new tube for storage at −80°C. Viral burden was measured by FFA. Briefly, tissue supernatants were serially diluted in DMEM with TPCK-Trypsin and applied to MDCK cell monolayers in a 96-well plate. After 1 h to allow virus adsorption, 2% methylcellulose was applied to prevent lateral viral spread. At 24 h after infection, cells were fixed with 4% paraformaldehyde and probed with anti-PR8 polyclonal mouse sera in permeabilization

buffer. After washing, an anti-mouse conjugated to horseradish peroxidase was applied. After washing, the FFA was developed by adding TrueBlue peroxidase substrate and imaged and counted using an ELIspot plate reader (Brien et al., 2019).

Peripheral P14 depletion

To deplete peripheral P14 cells while preserving P14 cells within tissues, mice were administered 0.05 µg of anti-CD90.1 (clone 19E12) IP route three times every other day. To confirm depletion, peripheral blood was collected from each mouse 1 day after the final antibody dose and screened via flow cytometry. A subset of animals was euthanized to assess depletion in the spleen and lungs.

mRNA vaccine construct

An expression cassette encoding A76 mutant ubiquitin (which prevents transient ubiquitin cleavage) (Rodriguez et al., 1997), followed by a flexible linker and the IAV H-2^b restricted T cell epitopes NP_{366} and PA_{224} and the LCMV epitope GP_{33}, each flanked by the optimal proteasomal cleavage sequence (Rodriguez et al., 1997; Finch et al., 1990), was cloned into a pmRNAxp expression plasmid (cat. #MR000PA-1; System Biosciences). In vitro mRNA production was driven by a type II T7 promoter element and cotranscriptionally capped and polyadenylated using an NEB-ARCA T7 kit supplemented with 50% ψUTP and 5mCTP. RNA was purified using a Qiagen RNeasy kit according to the manufacturer's instructions. mRNA was packaged into LNPs using a Precigenome Nanogenerator Flex microfluidics device. Briefly, the mRNA-containing aqueous phase was rapidly mixed with the lipid-containing organic phase at a flow rate ratio of 3:1 (aqueous:organic phase) and a total flow rate of 3 ml/min using a micromixer chip (cat. #CHP-MIX-4; Precigenome) and a commercial microfluidic mixing system (NanoGenerator Flex; Precigenome). The LNP was then purified and concentrated by ultracentrifugation. The aqueous phase was prepared by diluting the mRNA in 50-mM sodium acetate buffer (pH 5.0). The organic phase was prepared by diluting a commercial neutral lipid mixture (cat. #PG-SYN-LF1ML, LipidFlex; Precigenome) in ethanol (99.5%) and supplemented with SM-102 ionizable lipid at a molar ratio of 6:4. The N/P ratio of the LNP formulation was fixed at 6 for all mRNA preparations. LNP size was confirmed to be 90–125 nm dynamic light scattering (Zetasizer Nano ZS; Malvern Analytical). The concentration of encapsulated RNA was measured using a Ribogreen encapsulation assay (Rosenblum et al., 2020). Mice were vaccinated with 5 µg of encapsulated RNA in the right quadriceps. As a negative control, mice were administered encapsulated RNA encoding GFP and a scrambled nucleotide sequence of the same epitopes such that no immunogenic peptides were formed.

Statistical analysis

Statistical analysis was performed using GraphPad Prism software. For comparisons between three and four groups, an ANOVA statistical test was utilized to determine statistical significance. For comparisons between two groups, a Mann–Whitney test was utilized to determine statistical significance. Experiments were repeated at least two times with an n of ≥ 5 animals per group. Statistical significance has been indicated within the figures with asterisks (*P = 0.03, **P = 0.002, ***P = 0.0002, ****P < 0.0001).

Online supplemental material

Fig. S1 demonstrates the gating strategy for lung T_{RM} and splenic T_{CM} and T_{EM}. Panels C–F numerically quantify splenic CD8$^+$, P14, and P14 T_{CM} and T_{EM} cells over time after radiation exposure. Fig. S2 demonstrates the validity of peripheral P14 depletion. On day 1, following administration of low-dose (0.03 µg) anti-thy1.1-depleting antibody, peripheral blood was collected and stained to quantify P14 cells. Additionally, lungs were harvested to determine that the dose of anti-thy1.1 was not sufficient to deplete lung T_{RM}. Fig. S3 demonstrates that the use of a peripherally replicating recombinant pathogen (LM expressing GP33) is sufficient to drive recovery of P14 T_{RM} in the lung following thorax-targeted radiation exposure.

Data availability

Requests for data should be directed to and will be fulfilled by the corresponding author.

Acknowledgments

The authors would like to acknowledge Amanda Kalen, Aimee Butler, and Dr. Vahid Nasirian of the Free Radical and Radiation Biology Program at the University of Iowa (Iowa City, IA, USA) for their assistance with operating the Xstrahl SARRP. Research reported in this publication was supported by the National Cancer Institute of the NIH under award number P30CA086862. The authors would like to thank the Kevin Legge Lab at the University of Iowa (Iowa City, IA, USA) and the NIH tetramer core facility for providing tetramer reagents.

This work was supported by grants from the NIH National Institute of Allergy and Infectious Diseases (AI42767, AI178159, AI167847 to J.T. Harty, AI114543 to J.T. Harty and V.P. Badovinac, GM134880 to V.P. Badovinac); NIH (R21 EY034198-01, R21ES032937-01A1, R21 DE031042-01A1, 2P30CA086862), the National Science Foundation (2242763) to A.K. Salem and P. Phruttiwanichakun; the Lyle and Bighley Chair of Pharmaceutical Sciences to A.K. Salem; NIH-funded T32 AI007260 and 1F32AI174382 to M. Hassert; Environmental Health Sciences Research Center (P30ES005605) to A.K. Salem and R. He; NIH-funded T32 GM007337 and a University of Iowa Graduate College Post-Comprehensive Research Fellowship to M.R. Mix.

Author contributions: Conceptualization: M. Hassert, J.T. Harty, and V.P. Badovinac; Data Curation: M. Hassert; Formal Analysis: M. Hassert; Investigation: M. Hassert, M. Hassert, and L.L. Pewe; Methodology: M. Hassert, R. He, M. Hassert, P. Phruttiwanichakun, S. van de Wall, and M.R. Mix; Funding Acquisition: M. Hassert, J.T. Harty, V.P. Badovinac, and A.K. Salem; Resources: J.T. Harty, V.P. Badovinac, and A.K. Salem; Visualization: MH; Writing (Original Draft) M. Hassert and J.T. Harty; Writing (Review and Editing): M. Hassert, A.K. Salem, M.R. Mix, J.T. Harty, and V.P. Badovinac; Project Administration: J.T. Harty, V.P. Badovinac, and A.K. Salem.

Disclosures: The authors declare no competing interests exist.

Submitted: 5 July 2023
Revised: 6 November 2023
Accepted: 31 January 2024

References

Anthony, S.M., N. Van Braeckel-Budimir, S.J. Moioffer, S. van de Wall, Q. Shan, R. Vijay, R. Sompallae, S.M. Hartwig, I.J. Jensen, S.M. Varga, et al. 2021. Protective function and durability of mouse lymph node-resident memory CD8+ T cells. *Elife*. 10:e68662. https://doi.org/10.7554/eLife.68662

Brauer, R., and P. Chen. 2015. Influenza virus propagation in embryonated chicken eggs. *J. Vis. Exp.* 52421. https://doi.org/10.3791/52421

Brien, J.D., M. Hassert, E.T. Stone, E. Geerling, L. Cruz-Orengo, and A.K. Pinto. 2019. Isolation and quantification of zika virus from multiple organs in a mouse. *J. Vis. Exp.* https://doi.org/10.3791/59632

Brown, D.M., A.M. Dilzer, D.L. Meents, and S.L. Swain. 2006. CD4 T cell-mediated protection from lethal influenza: Perforin and antibody-mediated mechanisms give a one-two punch. *J. Immunol.* 177:2888–2898. https://doi.org/10.4049/jimmunol.177.5.2888

Casey, K.A., K.A. Fraser, J.M. Schenkel, A. Moran, M.C. Abt, L.K. Beura, P.J. Lucas, D. Artis, E.J. Wherry, K. Hogquist, et al. 2012. Antigen-independent differentiation and maintenance of effector-like resident memory T cells in tissues. *J. Immunol.* 188:4866–4875. https://doi.org/10.4049/jimmunol.1200402

Cepek, K.L., S.K. Shaw, C.M. Parker, G.J. Russell, J.S. Morrow, D.L. Rimm, and M.B. Brenner. 1994. Adhesion between epithelial cells and T lymphocytes mediated by E-cadherin and the alpha E beta 7 integrin. *Nature*. 372:190–193. https://doi.org/10.1038/372190a0

Cytlak, U.M., D.P. Dyer, J. Honeychurch, K.J. Williams, M.A. Travis, and T.M. Illidge. 2022. Immunomodulation by radiotherapy in tumour control and normal tissue toxicity. *Nat. Rev. Immunol.* 22:124–138. https://doi.org/10.1038/s41577-021-00568-1

Fakiris, A.J., R.C. McGarry, C.T. Yiannoutsos, L. Papiez, M. Williams, M.A. Henderson, and R. Timmerman. 2009. Stereotactic body radiation therapy for early-stage non-small-cell lung carcinoma: Four-year results of a prospective phase II study. *Int. J. Radiat. Oncol. Biol. Phys.* 75:677–682. https://doi.org/10.1016/j.ijrobp.2008.11.042

Fernandez-Ruiz, D., W.Y. Ng, L.E. Holz, J.Z. Ma, A. Zaid, Y.C. Wong, L.S. Lau, V. Mollard, A. Cozijnsen, N. Collins, et al. 2016. Liver-resident memory CD8+ T cells form a front-line defense against malaria liver-stage infection. *Infect. Immun.* 45:889–902. https://doi.org/10.1016/j.immuni.2016.08.011

Finch, J.S., K. Bonham, P. Krieg, and G.T. Bowden. 1990. Murine polyubiquitin mRNA sequence. *Nucleic Acids Res.* 18:1907. https://doi.org/10.1093/nar/18.7.1907

Galluzzi, L., A. Buqué, O. Kepp, L. Zitvogel, and G. Kroemer. 2017. Immunogenic cell death in cancer and infectious disease. *Nat. Rev. Immunol.* 17:97–111. https://doi.org/10.1038/nri.2016.107

Gebhardt, T., L.M. Wakim, L. Eidsmo, P.C. Reading, W.R. Heath, and F.R. Carbone. 2009. Memory T cells in nonlymphoid tissue that provide enhanced local immunity during infection with herpes simplex virus. *Nat. Immunol.* 10:524–530. https://doi.org/10.1038/ni.1718

Grayson, J.M., Harrington, L.E., Lanier, J.G., Wherry, E.J. & Ahmed, R. 2002. Differential sensitivity of naive and memory CD8+ T cells to apoptosis in vivo. *J. Immunol.* 169:3760–3770. https://doi.org/10.4049/jimmunol.169.7.3760

Guipaud, O., C. Jaillet, K. Clément-Colmou, A. François, S. Supiot, and F. Milliat. 2018. The importance of the vascular endothelial barrier in the immune-inflammatory response induced by radiotherapy. *Br. J. Radiol.* 91:20170762. https://doi.org/10.1259/bjr.20170762

Hassert, M., and J.T. Harty. 2022. Tissue resident memory T cells- A new benchmark for the induction of vaccine-induced mucosal immunity. *Front. Immunol.* 13:1039194. https://doi.org/10.3389/fimmu.2022.1039194

Heidarian, M., I.J. Jensen, S.K. Kannan, L.L. Pewe, M. Hassert, S. Park, H.-H. Xue, J.T. Harty, and V.P. Badovinac. 2023. Sublethal whole-body irradiation induces permanent loss and dysfunction in pathogen-specific circulating memory CD8 T cell populations. *Proc. Natl. Acad. Sci. USA*. 120:e2302785120. https://doi.org/10.1073/pnas.2302785120

IEA-REPORTS. 2019. Nuclear power in a clean energy system. IEA, 4.0, Paris, France. https://doi.org/10.1787/fc5f4b7e-en

Jameson, S.C., and D. Masopust. 2018. Understanding subset diversity in T cell memory. *Immunity*. 48:214–226. https://doi.org/10.1016/j.immuni.2018.02.010

Jiang, X., R.A. Clark, L. Liu, A.J. Wagers, R.C. Fuhlbrigge, and T.S. Kupper. 2012. Skin infection generates non-migratory memory CD8+ T(RM) cells providing global skin immunity. *Nature*. 483:227–231. https://doi.org/10.1038/nature10851

Kirsch, D.G., J. Grimm, A.R. Guimaraes, G.R. Wojtkiewicz, B.A. Perez, P.M. Santiago, N.K. Anthony, T. Forbes, K. Doppke, R. Weissleder, and T. Jacks. 2010. Imaging primary lung cancers in mice to study radiation biology. *Int. J. Radiat. Oncol. Biol. Phys.* 76:973–977. https://doi.org/10.1016/j.ijrobp.2009.11.038

Kok, L., D. Masopust, and T.N. Schumacher. 2022. The precursors of CD8+ tissue resident memory T cells: From lymphoid organs to infected tissues. *Nat. Rev. Immunol.* 22:283–293. https://doi.org/10.1038/s41577-021-00590-3

Laidlaw, B.J., N. Zhang, H.D. Marshall, M.M. Staron, T. Guan, Y. Hu, L.S. Cauley, J. Craft, and S.M. Kaech. 2014. CD4+ T cell help guides formation of CD103+ lung-resident memory CD8+ T cells during influenza viral infection. *Immunity*. 41:633–645. https://doi.org/10.1016/j.immuni.2014.09.007

Liang, S., K. Mozdzanowska, G. Palladino, and W. Gerhard. 1994. Heterosubtypic immunity to influenza type A virus in mice. Effector mechanisms and their longevity. *J. Immunol.* 152:1653–1661. https://doi.org/10.4049/jimmunol.152.4.1653

Low, J.S., Y. Farsakoglu, M.C. Amezcua Vesely, E. Sefik, J.B. Kelly, C.C.D. Harman, R. Jackson, J.A. Shyer, X. Jiang, L.S. Cauley, et al. 2020. Tissue-resident memory T cell reactivation by diverse antigen-presenting cells imparts distinct functional responses. *J. Exp. Med.* 217:e20192291. https://doi.org/10.1084/jem.20192291

Low, J.S., and S.M. Kaech. 2018. Trials and Tribble-ations of tissue T_{RM} cells. *Nat. Immunol.* 19:102–103. https://doi.org/10.1038/s41590-017-0031-9

Luangrath, M.A., M.E. Schmidt, S.M. Hartwig, and S.M. Varga. 2021. Tissue-resident memory T cells in the lungs protect against acute respiratory syncytial virus infection. *Immunohorizons*. 5:59–69. https://doi.org/10.4049/immunohorizons.2000067

Martin, M.D., and V.P. Badovinac. 2018. Defining memory CD8 T cell. *Front. Immunol.* 9:2692. https://doi.org/10.3389/fimmu.2018.02692

Masopust, D., V. Vezys, A.L. Marzo, and L. Lefrançois. 2001. Preferential localization of effector memory cells in nonlymphoid tissue. *Science*. 291:2413–2417. https://doi.org/10.1126/science.1058867

Mueller, S.N., T. Gebhardt, F.R. Carbone, and W.R. Heath. 2013. Memory T cell subsets, migration patterns, and tissue residence. *Annu. Rev. Immunol.* 31:137–161. https://doi.org/10.1146/annurev-immunol-032712-095954

Mueller, S.N., W.A. Langley, G. Li, A. García-Sastre, R.J. Webby, and R. Ahmed. 2010. Qualitatively different memory CD8+ T cells are generated after lymphocytic choriomeningitis virus and influenza virus infections. *J. Immunol.* 185:2182–2190. https://doi.org/10.4049/jimmunol.1001142

Nabrinsky, E., J. Macklis, and J. Bitran. 2022. A review of the abscopal effect in the era of immunotherapy. *Cureus*. 14:e29620. https://doi.org/10.7759/cureus.29620

Perez, B.A., A.P. Ghafoori, C.-L. Lee, S.M. Johnston, Y. Li, J.G. Moroshek, Y. Ma, S. Mukherjee, Y. Kim, C.T. Badea, and D.G. Kirsch. 2013. Assessing the radiation response of lung cancer with different gene mutations using genetically engineered mice. *Front. Oncol.* 3:72. https://doi.org/10.3389/fonc.2013.00072

Rodriguez, F., J. Zhang, and J.L. Whitton. 1997. DNA immunization: Ubiquitination of a viral protein enhances cytotoxic T-lymphocyte induction and antiviral protection but abrogates antibody induction. *J. Virol.* 71:8497–8503. https://doi.org/10.1128/jvi.71.11.8497-8503.1997

Rosenblum, D., A. Gutkin, R. Kedmi, S. Ramishetti, N. Veiga, A.M. Jacobi, M.S. Schubert, D. Friedmann-Morvinski, Z.R. Cohen, M.A. Behlke, et al. 2020. CRISPR-Cas9 genome editing using targeted lipid nanoparticles for cancer therapy. *Sci. Adv.* 6:eabc9450. https://doi.org/10.1126/sciadv.abc9450

Rutigliano, J.A., S. Sharma, M.Y. Morris, T.H. Oguin III, J.L. McClaren, P.C. Doherty, and P.G. Thomas. 2014. Highly pathological influenza A virus infection is associated with augmented expression of PD-1 by functionally compromised virus-specific CD8+ T cells. *J. Virol.* 88:1636–1651. https://doi.org/10.1128/JVI.02851-13

Sakai, S., K.D. Kauffman, J.M. Schenkel, C.C. McBerry, K.D. Mayer-Barber, D. Masopust, and D.L. Barber. 2014. Cutting edge: Control of Mycobacterium tuberculosis infection by a subset of lung parenchyma-homing CD4 T cells. *J. Immunol.* 192:2965–2969. https://doi.org/10.4049/jimmunol.1400019

Slavin, S. 1987. Total lymphoid irradiation. *Immunol. Today*. 8:88–92. https://doi.org/10.1016/0167-5699(87)90852-8

Slütter, B., N. Van Braeckel-Budimir, G. Abboud, S.M. Varga, S. Salek-Ardakani, and J.T. Harty. 2017. Dynamics of influenza-induced lung-resident memory T cells underlie waning heterosubtypic immunity. *Sci. Immunol.* 2:eaag2031. https://doi.org/10.1126/sciimmunol.aag2031

Teijaro, J.R., D. Verhoeven, C.A. Page, D. Turner, and D.L. Farber. 2010. Memory CD4 T cells direct protective responses to influenza virus in the lungs through helper-independent mechanisms. *J. Virol.* 84: 9217–9226. https://doi.org/10.1128/JVI.01069-10

Ukleja, J., E. Kusaka, and D.T. Miyamoto. 2021. Immunotherapy combined with radiation therapy for genitourinary malignancies. *Front. Oncol.* 11: 663852. https://doi.org/10.3389/fonc.2021.663852

Van Braeckel-Budimir, N., S.M. Varga, V.P. Badovinac, and J.T. Harty. 2018. Repeated antigen exposure extends the durability of influenza-specific lung-resident memory CD8$^+$ T cells and heterosubtypic immunity. *Cell Rep.* 24:3374–3382.e3. https://doi.org/10.1016/j.celrep.2018.08.073

Wakim, L.M., A. Woodward-Davis, and M.J. Bevan. 2010. Memory T cells persisting within the brain after local infection show functional adaptations to their tissue of residence. *Proc. Natl. Acad. Sci. USA.* 107: 17872–17879. https://doi.org/10.1073/pnas.1010201107

Wilk, M.M., A. Misiak, R.M. McManus, A.C. Allen, M.A. Lynch, and K.H.G. Mills. 2017. Lung CD4 tissue-resident memory T cells mediate adaptive immunity induced by previous infection of mice with *Bordetella pertussis*. *J. Immunol.* 199:233–243. https://doi.org/10.4049/jimmunol.1602051

Wu, T., Y. Hu, Y.T. Lee, K.R. Bouchard, A. Benechet, K. Khanna, and L.S. Cauley. 2014. Lung-resident memory CD8 T cells (TRM) are indispensable for optimal cross-protection against pulmonary virus infection. *J. Leukoc. Biol.* 95:215–224. https://doi.org/10.1189/jlb.0313180

Yewdell, J.W., J.R. Bennink, G.L. Smith, and B. Moss. 1985. Influenza A virus nucleoprotein is a major target antigen for cross-reactive anti-influenza A virus cytotoxic T lymphocytes. *Proc. Natl. Acad. Sci. USA.* 82: 1785–1789. https://doi.org/10.1073/pnas.82.6.1785

Zhang, Z., J. Zhou, V. Verma, X. Liu, M. Wu, J. Yu, and D. Chen. 2021. Crossed pathways for radiation-induced and immunotherapy-related lung injury. *Front. Immunol.* 12:774807. https://doi.org/10.3389/fimmu.2021.774807

Supplemental material

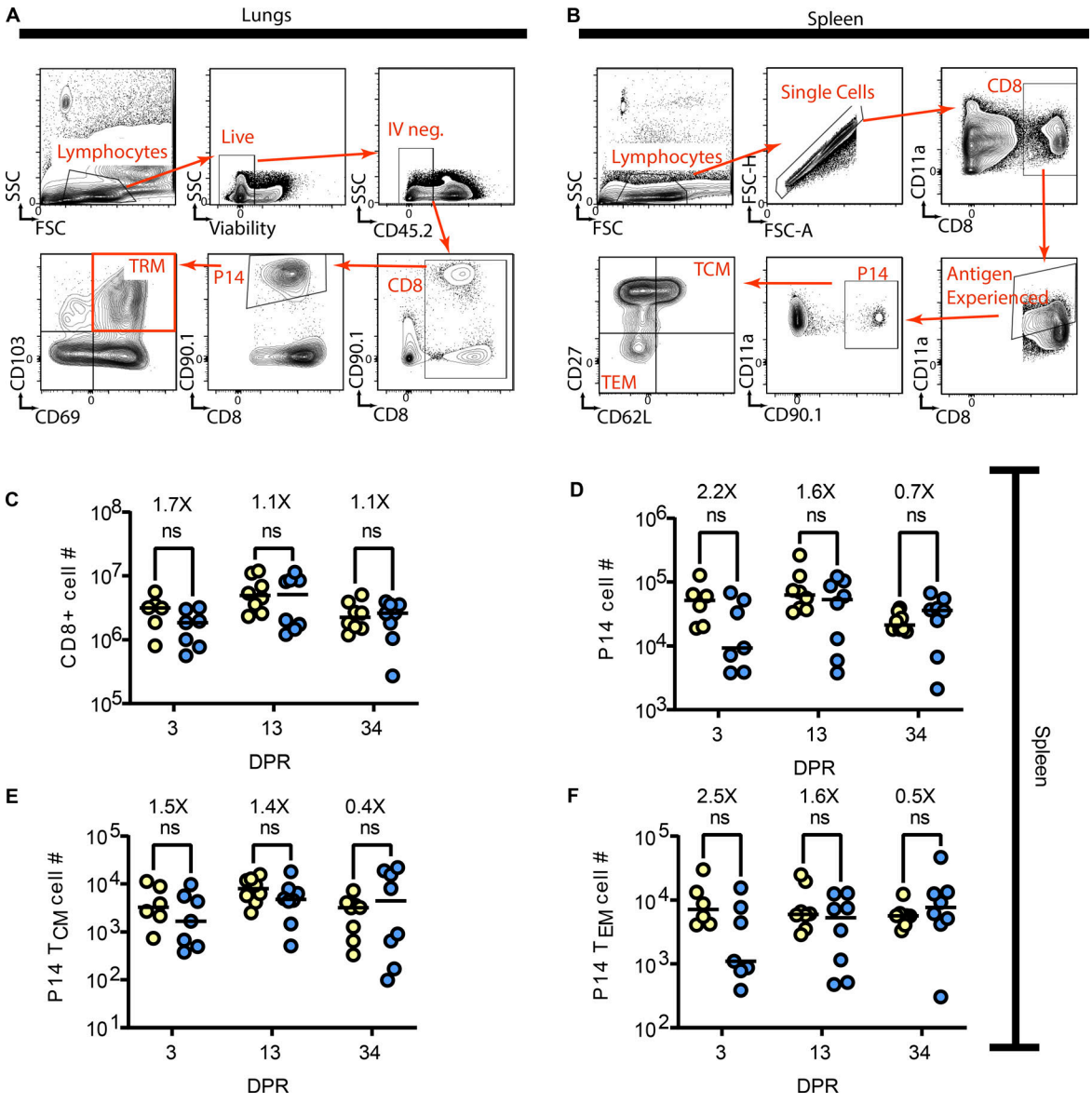

Figure S1. **Gating strategies for T_{RM}, T_{CM}, and T_{EM}.** 3 min prior to euthanasia, mice were administered 2 µg of BV421 labeled anti-CD45.2 to discriminate vascular from tissue cells. **(A)** For lung T_{RM}, cells were gated on lymphocytes, live, and IV-negative cells that express CD8, followed by CD90.1 to identify P14 cells. Lung T_{RM} are identified as being double positive for CD69 and CD103. **(B)** Splenocytes were gated on lymphocytes, single cells that are $CD8^+$. CD11a is used to identify antigen-experienced cells, which are then further subset into P14 cells using CD90.1. T_{CM} and T_{EM} are differentiated using CD62L and CD27. **(C–F)** Flow cytometric analysis was utilized on whole spleens to enumerate the total number of (C) $CD8^+$ T cells, (D) P14 cells, (E) T_{CM} P14 cells, and (F) T_{EM} P14 cells. ANOVA was utilized to determine statistically significant differences between groups. Data are pooled from two independent experiments (n = 6–7).

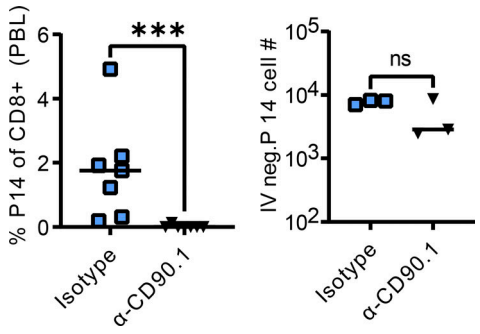

Figure S2. **Circulating P14 depletion confirmation.** Prior to PR8-GP33 infection, blood was collected from each mouse, stained, and analyzed via flow cytometry to determine the depletion efficiency of peripheral P14 cells. The dose of anti-CD90.1 was confirmed to not deplete lung T_{RM}. Mann–Whitney test was utilized to determine statistically significant differences between groups. The data are pooled from two independent experiments (*n* = 3–6 per group). Statistical significance has been indicated within the figures with asterisks (***P = 0.0002).

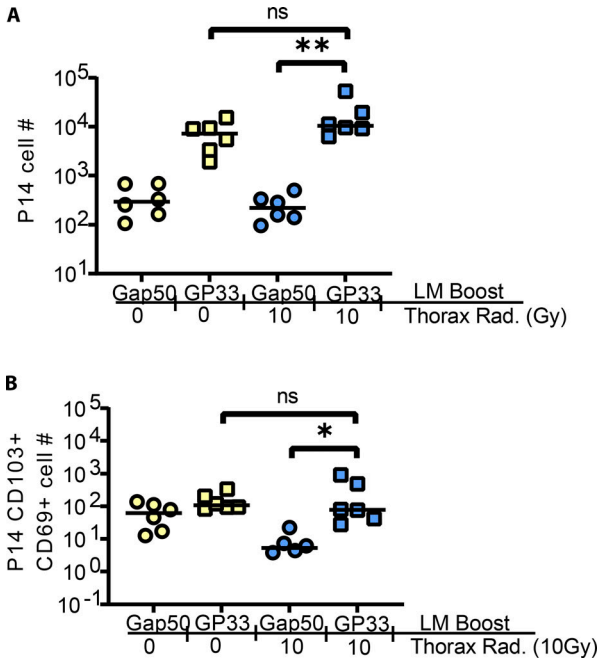

Figure S3. **LM-GP33 peripheral infection results in T_{RM} regeneration following radiation-induced loss.** Mice were administered P14 1 day prior to infection of half of the mice with X31-GP33. 30 DPPI, half of the mice were exposed to 10 Gy of thorax-targeted radiation or treated similarly without radiation exposure. 14 DPR, mice were infected IV with a LM-GP33 boost or LM-Gap50 as a negative control. 30 days after secondary infection, mice were humanely euthanized and lungs and spleens were harvested for flow cytometry. **(A and B)** Flow cytometric analysis was utilized to count the total number of (A) IV-negative P14 cells in the lungs and (B) P14 lung T_{RM}. ANOVA was utilized to determine statistically significant differences between groups. Data are pooled from two independent experiments (*n* = 6 per group). Statistical significance has been indicated within the figures with asterisks (*P = 0.03, **P = 0.002).